Digestive Diseases and Sciences (2020) 65:3521–3537
https://doi.org/10.1007/s10620-020-06140-6

ORIGINAL ARTICLE

Teduglutide Promotes Epithelial Tight Junction Pore Function in Murine Short Bowel Syndrome to Alleviate Intestinal Insufficiency

Johannes Reiner[1] · Peggy Berlin[1] · Jakob Wobar[1] · Holger Schäffler[1] · Karen Bannert[1] · Manuela Bastian[2] · Brigitte Vollmar[3] · Robert Jaster[1] · Georg Lamprecht[1] · Maria Witte[4]

Received: 13 December 2019 / Accepted: 9 February 2020 / Published online: 19 February 2020

Abstract

Background In short bowel syndrome, epithelial surface loss results in impaired nutrient absorption and may lead to intestinal insufficiency or intestinal failure. Nucleotide oligomerization domain 2 (Nod2) dysfunction predisposes to the development of intestinal failure after intestinal resection and is associated with intestinal barrier defects. Epithelial barrier function is crucial for intestinal absorption and for intestinal adaptation in the short bowel situation.

Aims The aim of the study was to characterize the effects of the GLP-2 analogue Teduglutide in the small intestine in the presence and absence of Nod2 in a mouse model of short bowel syndrome.

Methods Mice underwent 40% ICR and were thereafter treated with Teduglutide versus vehicle injections. Survival, body weight, stool water, and sodium content and plasma aldosterone concentrations were determined. Intestinal and kidney tissue was examined with light and fluorescence microscopy, Ussing chamber studies and quantitative PCR in wild type and transgenic mice.

Results Teduglutide reduced intestinal failure incidence in Nod2 k.o. mice. In wt mice, Teduglutide attenuated intestinal insufficiency as indicated by reduced body weight loss and lower plasma aldosterone concentrations, lower stool water content, and lower stool sodium losses. Teduglutide treatment was associated with enhanced epithelial paracellular pore function and enhanced claudin-10 expression in tight junctions in the villus tips, where it colocalized with sodium–glucose cotransporter 1 (SGLT-1), which mediates Na-coupled glucose transport.

Conclusions In the SBS situation, Teduglutide not only maximizes small intestinal mucosal hypertrophy but also partially restores small intestinal epithelial function through an altered distribution of claudin-10, facilitating sodium recirculation for Na-coupled glucose transport and water absorption.

Keywords Short bowel syndrome · Mouse model · Ussing chamber · Teduglutide · Barrier function · Nucleotide oligomerization domain 2

Abbreviations

GLP-2	Glucagon-like peptide 2
Nod2	Nucleotide oligomerization domain 2
RAAS	Renin–angiotensin–aldosterone system
PS	Parenteral support

Introduction

Short bowel syndrome occurs after major intestinal resection and may cause intestinal insufficiency or intestinal failure (IF) [1]. Resection-associated intestinal adaptation compensates for the reduced absorptive mucosal surface area and may involve hyperphagia, polydipsia, prolonged gastrointestinal transit time, absorptive surface area expansion, increased epithelial transport, and increased mesenteric blood flow [2, 3]. Besides macronutrient malabsorption, high intestinal salt and water losses are the major challenge to achieve oral autonomy. Severe resection-associated salt and water depletion, which occurs when intestinal adaptation is insufficient, may activate the renin–angiotensin–aldosterone system (RAAS) in these patients [4]. If adaptation is not sufficient to maintain

✉ Georg Lamprecht
georg.lamprecht@med.uni-rostock.de

Extended author information available on the last page of the article

health or growth, chronic intestinal insufficiency ensues and may even lead to IF that requires organ replacement therapy, i.e., long-term parenteral nutrition [5].

In mice, extensive ileocecal resection leads to intestinal insufficiency as a compensated state or intestinal failure (IF) as a decompensated state that will lead to death because mice cannot be parenterally supplemented.

Nucleotide-binding oligomerization domain-containing protein 2 (NOD2) dysfunction is a well-known risk factor for the development of Crohn's disease [6–8]. In addition, it is a risk factor for insufficient adaptation and intestinal failure, independent of the underlying disease [9, 10]. We have recently reported that extensive ileocecal resection induces severe intestinal failure in Nod2 knockout mice compared to wt mice through mechanisms involving impaired epithelial barrier function and microbiome alterations [11].

One mechanism of intestinal adaptation is GLP-2-stimulated mucosal growth [12]. Teduglutide is a stable analogue of glucagon-like peptide 2 (GLP-2) and reduces parenteral support (PS) in chronic IF. A GLP-2-dependent growth effect on the remaining small bowel mucosa is well described in SBS [13, 14]. Although villus hypertrophy implies some gain of absorptive cell mass, the increment in villus length does not translate numerically equal into functional measures such as wet weight absorption [13]. Also, spontaneous villus elongation does not correlate with functionally effective adaptation [15].

Intestinal barrier function is essential for vectorial transport, and GLP-2 has been reported to effect tight junction protein expression in healthy animals [16]. To test the effects of GLP-2 agonism on epithelial barrier function in the SBS epithelium, Teduglutide effects were studied in a mouse model of intestinal insufficiency secondary to extensive ileocecal resection, mimicking the most prevalent situation of human SBS [17]. This is of particular relevance because the resection of ileum and cecum removes a large pool of GLP-2-secreting L-cells and thus represents substantial loss of GLP-2 secretory capacity [18].

Teduglutide is particularly efficient in severe SBS in humans [19], and Nod2 deficiency is associated with severe SBS in humans and mice, but it is unknown whether Nod2 interferes with Teduglutide's mechanism of action. To further test the effects of Teduglutide in SBS, it was tested in wt and in Nod2 k.o. mice after extensive ICR as a model of intestinal insufficiency and intestinal failure.

Methods

Mice

For all experiments, C57BL6/J (wt) mice and B6.129S1-Nod2tm1Flv/J stock #005763 (Nod2 knockout, k.o.) [20] were purchased from Jackson Laboratory (Bar Harbor, USA) and bred in the animal facilities at the Rudolf-Zenker-Institute for Experimental Surgery, University Medical Center Rostock. Genotyping for the Nod2tm1Flv allele was performed with standard PCR procedures as described previously [11]. Mice were housed in groups of up to five under conventional conditions with free access to standard chow and water until surgery. Adult, male mice of ~30 g body weight with the age of ~4 months received 12-cm ileum and cecum resection (ICR) and were then randomly assigned to either Teduglutide or vehicle treatment. To prevent intestinal obstruction, all mice were switched to liquid diet (AIN 93G, Ssniff, Soest, Germany) 2 days before surgery and maintained on this diet until the end of the experiment. Feeds were replenished daily. All mice were studied/followed with the intention to survive to day 14.

Humane Endpoints

A wellness score below 4 points, body weight loss of more than 20% from the initial weight, a distended abdomen together with persistent constipation or signs of dehydration combined with massive diarrhea were defined as humane endpoints. Mice that reached one or more humane endpoints were killed immediately and underwent autopsy.

Procedures

Briefly, mice were anesthetized by i. p. injection of ketamine (100 mg/kg bw) and xylazine (15 mg/kg bw) and orally intubated and ventilated as described previously [15]. After midline incision, the distal small bowel and the cecum were exposed and then transected 12 cm proximal to the ileocecal junction and immediately distal to the cecum. The resected bowel was removed, and the length of the specimen was measured. An end-to-end, full-thickness jejuno-colonic anastomosis was created as described previously. Immediately after surgery, all mice were weighted and received 1 ml isotonic saline subcutaneously and 5 mg/kg body weight carprofen. All surgical procedures were performed by the same surgeon (MW). Mice recovered in a heated terrarium (29 °C) for 4 h and then returned to individual cages with free access to liquid food and water. From day 1 after surgery, mice were injected twice daily with 0.1 mg/kg body weight Teduglutide (Shire-NPS Pharmaceuticals, Inc., Lexington, MA, USA,), a dose that had previously been used in mice [16]. PBS served as vehicle control.

Clinical Parameters

Body weight, wellness score [21], stool water, and aldosterone plasma concentrations were analyzed as described previously [15]. In brief, mice were weighed and scored

daily using a previously, for this model, verified wellness score with 8 items. For determination of stool water content and stool sodium, stool was collected before surgery (day 0) and on postoperative days 2, 7, and 14. For that, mice were individually placed in an empty cage covered with tissue paper (WEPA Professional GmbH, Germany) and observed for 30 min. Stool was collected immediately after excretion using cotton swabs and placed in a preweighed empty 2.0-ml Eppendorf tube. The tube with fresh stool was immediately weighed, dried overnight at 80 °C, and then weighed with exsiccated stool. Water content was then calculated as before [15]. These exsiccated stools were then used for determination of sodium concentrations. Stool sodium was measured after 5 × dilution with dH_2O with a Horiba LAQUA twin B-722 sodium meter and sampling sheets using the sampling sheet holder cover.

Histology

In total, 1-cm intestinal segments were immediately placed in MorFFFix (Morphisto®, Frankfurt am Main, Germany) for 24 h and then paraffin-embedded as described [15]. In total, 5-µm sections were HE-stained and then used for morphometric analysis. In a blinded manner, 5 well-oriented full-length villi per sample was measured using an Axio Observer inverted microscope (Zeiss) and ZEN 2.3 software.

Immunofluorescence

In total, 1-cm intestinal segments or kidneys were placed in Tissue-Tek® O.C.T.™, snap frozen in liquid nitrogen, wrapped in aluminum foil, and stored at − 80 °C for further use. In total, 5-µm-thick, longitudinal cryosections were cut on a CM 1850 cryotome (Leica Microsystems Nussloch GmbH, Nussloch, Germany) at − 20 °C. After a brief PBS wash, tissues were fixed with ice-cold acetone for 5 min at 4 °C. Tissue was then blocked with 10% fecal calf serum (FCS) for 60 min and incubated with primary antibodies (see Table 1) overnight at 4 °C. After 5 × 5 min PBS/1% FCS washes, secondary antibodies were incubated for 60 min at room temperature. After another 5x5 min washes and counterstaining with DAPI (Sigma-Aldrich, St. Louis, MO, USA, #D9542) tissues were mounted in fluorescence mounting medium (Dako North America Inc, Carpinteria, CA, USA, #S3023). Slides were imaged on a Zeiss Axio Observer (Zeiss, Oberkochen, Germany) equipped with an Apotome unit using Zen Software 2.3 software. Image analysis was performed using ImageJ2 [22]. Specifically, relative quantification of the claudin immunofluorescence signal along the villus surface was performed with a pixel line scan using the profiling tool of ImageJ2. The distance from villus base to villus tip along the line scan was set to 100% for each villus. The intensity of the claudin signal was normalized by the intensity of the F-actin signal. For semiquantitative analysis in the kidney collecting duct cells, pixel line scans were performed with the same profiling tool.

Table 1 Primary and secondary antibodies for this study

Antibody	Company	Catalog no.
Claudin-10 polyclonal antibody Rb/IgG	Invitrogen	38-8400
ENaC polyclonal antibody Rb/IgG	abcam	ab77385
AQP2 antibody (E-2) Alexa Fluor® 594	Santa Cruz	sc-515770
Alexa Fluor® 594 phalloidin	Invitrogen	A12381
Alexa Fluor® 488 goat antirabbit IgG (H + L)	Invitrogen	A11008
SGLT-1 polyclonal antibody Rb/IgG	abcam	ab14686

RNA Isolation and cDNA Synthesis

RNA was isolated as described previously [23]. Briefly, ~ 30 mg frozen tissue was mechanically disrupted in lysis buffer by 50 Hz for 5 min using a bead mill (TissueLyser LT, Qiagen, Hilden, Germany) with 7-mm stainless steel beads (Qiagen, Hilden, Germany). RNA isolation was performed with RNeasy Mini Kits (Qiagen, Hilden, Germany). At room temperature, 15-min DNA digestion was performed with the RNase-free DNase set (Qiagen, Hilden, Germany). Agarose gel electrophoresis was performed as quality control. cDNA synthesis was performed with 2 µg RNA, using the High-Capacity cDNA Reverse Transcription Kit (Thermo Fisher Scientific, Schwerte, Germany).

Quantitative Real-Time PCR

Gene expression of ion transporters and barrier proteins was analyzed by quantitative real-time PCR using TaqMan™ Universal PCR Master Mix and pre-designed TaqMan® gene expression assays (Table 2). In total, 15 ng cDNA was used for the PCR. Analyses were performed in triplicate on a ViiA7 sequence detection system (Applied Biosystems, USA). PCR conditions were as follows: 95 °C for 10 min, 55 cycles of 15 s at 95 °C, 1 min at 60 °C. The expression levels of the genes of interests are given as the difference to the housekeeping gene β-actin (ΔCt). Relative gene expression values are expressed as $2^{-\Delta\Delta Ct}$ at day 14 compared to day 0.

Ussing Chamber

Mouse jejunum was preincubated in ice-cold recording buffer containing 1 µM indomethacin for 10 min. The tissue was then freed from the seromuscular layer under a dissecting microscope and analyzed in Ussing chambers with a 5-ml half-cell volume and 0.24 cm^2 surface area with AgCl electrodes (Karl Mussler, Scientific Instruments, Germany)

Table 2 TaqMan probes for this study

Target gene	Company	Accession no.
cldn2	ThermoFisher	Mm00516703_s1
cldn3	ThermoFisher	Mm00515499_s1
cldn4	ThermoFisher	Mm00515514_s1
cldn7	ThermoFisher	Mm00516817_m1
cldn10	ThermoFisher	Mm01226326_g1
cldn15	ThermoFisher	Mm00517635_m1
ocln	ThermoFisher	Mm00500912_m1
tjp1	ThermoFisher	Mm00493699_m1
tjp2	ThermoFisher	Mm00495620_m1
gapdh	ThermoFisher	Mm99999915_g1
glp2r	ThermoFisher	Mm01329475_m1
actb	ThermoFisher	Mm00607939

as described previously [15]. Recording buffer contained 115 mM NaCl, 0.4 mM Na_2HPO4, 2.4 mM NaH_2PO_4, 5 mM KCl, 1.2 mM $MgCl_2$, 1.2 mM $CaCl_2$, 25 mM $NaHCO_3$, and 5 mM glucose, pH 7.4 and was continuously gassed with 95% O_2 and 5% CO_2 at 37 °C. Na/Cl dilution potentials were recorded after replacing 57.5 mM NaCl with 115 mM mannitol in the basolateral buffer. P_{Na}/P_{Cl} was calculated applying the Goldman-Hodgkin-Katz equation. Biionic potentials were performed with methylammoniumchloride, ethylammoniumchloride, tetramethylammoniumchloride, tetraethylammoniumchloride, and N-methyl-D-glucamin (NMDG). Mucosal to serosal FITC-4-kDa dextran flux was measured by adding it at 40 ng/ml into the mucosal compartment [24]. Fluorescence intensity increase in the serosal chamber was measured after 1 and 2 h using a Microplate reader (Glomax® # 9301-010, Promega, Fitchburg, WI, USA). Dextran flux was calculated from a simultaneously determined standard curve.

Statistical Analysis

All clinical data were recorded in a prospectively maintained database (Microsoft Access, Microsoft Corporation, Redmont, WA, USA). Statistical analysis was performed with GraphPad PRISM (GraphPad software, Inc., San Diego, CA, USA). All mice were operated with the intention to survive day 14. Mice that died before day 14 were excluded from all analyses except the survival analysis. Gaussian distribution was evaluated with the Kolmogorov–Smirnov test. Parametric data were analyzed with unpaired *t* test and paired *t* test where appropriate. Nonparametric data were analyzed with the Mann–Whitney *U* test. For multiple group comparisons, one- or two-way ANOVA was performed as indicated.

Study Approval

All animal experiments were performed according to the EU Directive 2010/63/EU of the animal protection act and approved by the local governmental administration (Landesamt für Landwirtschaft, Lebensmittelsicherheit und Fischerei Mecklenburg-Vorpommern, 7221.3-1.1-008/16).

Results

Teduglutide Prevents Intestinal Failure in Nod2 k.o. Mice and Alleviates Intestinal Insufficiency in wt Animals

To simulate severe SBS at the edge between intestinal insufficiency and intestinal failure, extensive ileocecal resection was performed in wt and Nod2 k.o. mice (Fig. 1a) and mice were followed for 14 days. From day 1 postoperatively, mice received subcutaneous injections of vehicle or Teduglutide, respectively (Fig. 1b). Resection length, remaining small bowel, and colon length were similar in all groups (Fig. 1c). Equal remnant lengths indicate that Teduglutide did not induce longitudinal growth. Vehicle-treated Nod2 k.o. mice had the lowest 14-day survival (44.0%, $n = 11/25$), reflecting the highest incidence of fatal intestinal failure. Strikingly, the Teduglutide-treated Nod2 k.o. cohort had significantly higher survival (86.7%, $n = 13/15$, $p < 0.05$, log-rank, Fig. 1d). Thus, Teduglutide prevents death from intestinal failure in Nod2 k.o. mice which suffer from particularly severe intestinal insufficiency. In wt animals, day 14 survival was similar in Teduglutide-treated and control animals (69.6%, 16/23 vs. 68.5%, 13/19, $p > 0.05$, log-rank, Fig. 1d), which suffer from less severe intestinal insufficiency than the Nod2 k.o. mice [11]. SBS-mediated body weight loss was significantly attenuated in the Teduglutide-treated wt animals ($91.1 \pm 1.8\%$ wt Teduglutide vs. $84.1 \pm 2.3\%$ wt vehicle, day 14, Fig. 1e). In Nod2 k.o. animals, no statistically significant difference was detectable for body weight at day 14 ($86.5 \pm 2.4\%$ Teduglutide vs. $82.9 \pm 2.2\%$ vehicle, Fig. 1e). Wellness score was similar between the groups at day 14 (10.7 vs. 10.5 and 10.2 vs. 9.9, $p > 0.05$, Fig. 1f) although the wellness score was at all times lower for Nod2 k.o. mice, independent of Teduglutide treatment. Thus, in the setting of intestinal insufficiency in wt mice, Teduglutide improves nutritional status as measured by body weight course. In the setting of intestinal insufficiency on the edge to intestinal failure in Nod2 k.o. mice, Teduglutide prevents decompensation to early death.

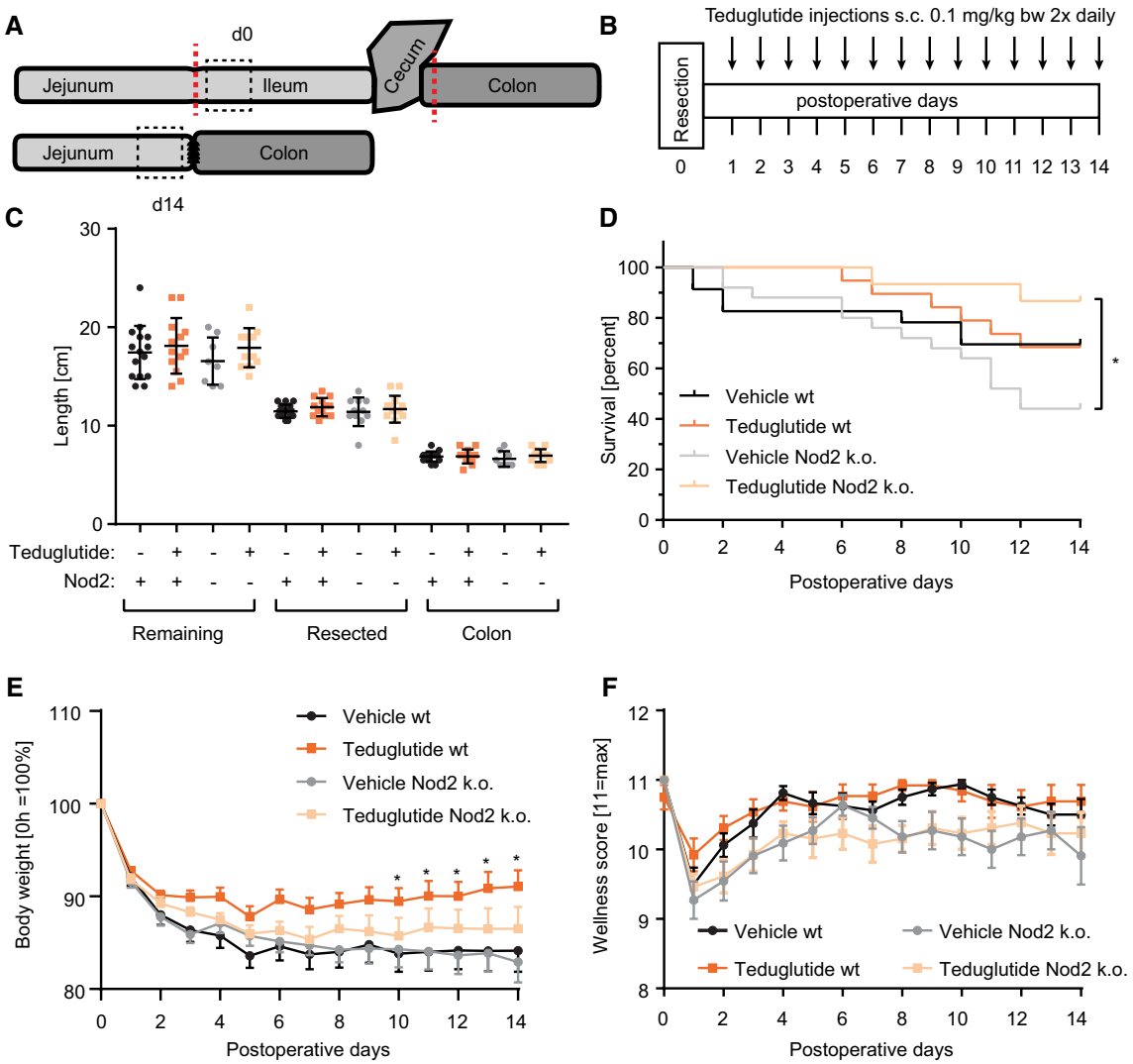

Fig. 1 Teduglutide prevents intestinal failure in Nod2 k.o. mice and intestinal insufficiency in wt mice. **a** 40% ileum plus cecum resection was performed. For all experiments, the segment distal to the resection margin was analyzed at day 0. At day 14, the segment proximal to the resection margin was analyzed. **b** Wt and Nod2 k.o. animals received Teduglutide in a dose of 0.1 mg/kg twice daily. This was compared to vehicle injections twice daily. **c** Resection and remaining bowel length of the different cohorts. Mean ± SD. **d** Survival plots for wt mice [14-day survival: vehicle in black vs. Teduglutide in orange, 68.5% (13/19) vs. 69.6% (16/23), $p > 0.05$, log-rank] and Nod2 k.o. animals [14-day survival: vehicle in gray vs. Teduglutide in light orange, 44.0% (11/25) vs. 86.7% (13/15), $p < 0.05$, log-rank]. **e** Body weight course of the different per protocol cohorts in percent of day 0, $^*p < 0.05$, Teduglutide wt versus vehicle wt, 2-way ANOVA, mean ± SEM, two-way ANOVA, corrected for multiple testing with two-stage step-up method of Benjamini, Krieger, and Yekutieli. **f** Wellness score course of the different cohorts, mean ± SEM, no significant differences

Teduglutide Reduces Stool Water Content and Stool Sodium Losses

Stool water content was increased at day 2 after surgery, independent of Teduglutide treatment in both wt and Nod2 k.o. animals (Fig. 2a, b). In wt animals, stool water content was significantly lower in the Teduglutide-treated than in the vehicle-injected group at day 7. At day 14, a trend to lower stool water content was notable in the Teduglutide-treated wt animals ($p = 0.20$). In Nod2 k.o. animals, no significant effect on stool water content was detectable. Stool sodium concentration did not change throughout the experiment and was not influenced by Teduglutide both in wt and in Nod2 k.o. animals (Fig. 2c, d). While stool volume was not measured in these mice, increased stool water content strongly suggests that increased stool output is accompanied by increased sodium losses, which are being reduced by Teduglutide treatment.

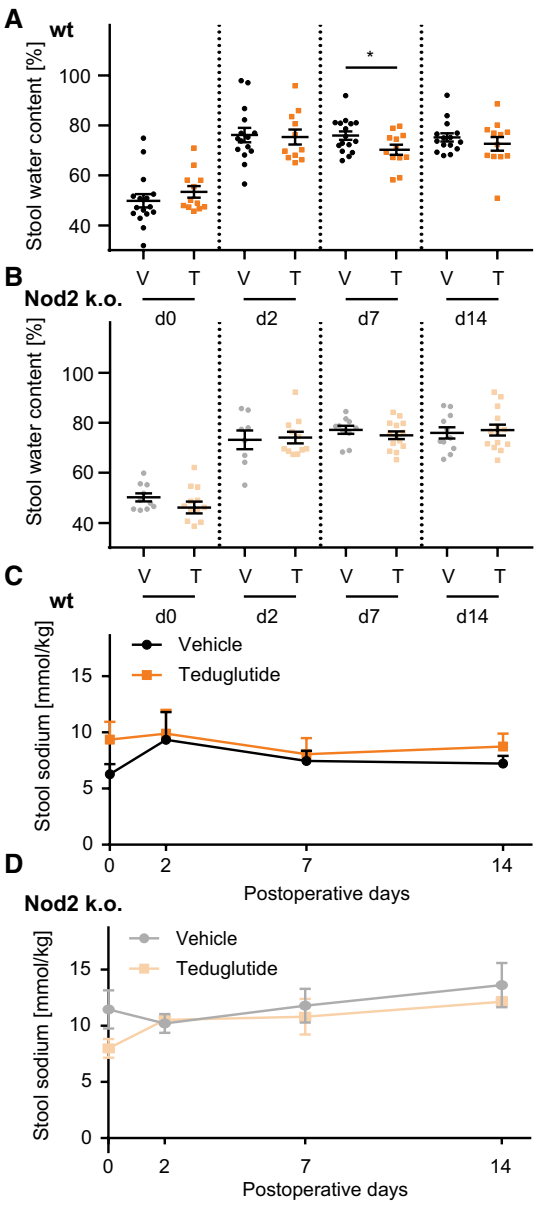

Fig. 2 Teduglutide reduces stool water and sodium losses. **a** Stool water content of wt animals over time. Mean ± SEM, $n = 16$ versus $n = 12$. Stool water content was significantly lower in Teduglutide-treated animals at day 7 (mean ± SEM: 75.9 ± 1.7%, vs. 70.3 ± 2.0%, $p < 0.05$, unpaired t test). **b** Stool water content of Nod2 k.o. animals over time. Mean ± SEM, $n = 10$ versus $n = 14$. Stool water content was not altered in Teduglutide-treated Nod2 k.o. mice at day 7 (mean ± SEM: 77.2 ± 1.6% vs. 75.0 ± 1.5%, $p > 0.05$, unpaired t test). **c** Stool sodium concentrations were unchanged over time in wt animals and not altered under Teduglutide treatment (mean ± SEM: day 0: 6.3 ± 2.6 mmol/kg vs. 9.4 ± 3.9 mmol/kg, $p > 0.05$, day 7: 7.5 ± 2.4 mmol/kg vs. 8.1 ± 2.9 mmol/kg, $p > 0.05$, day 14: 7.2 ± 1.7 mmol/kg vs. 8.7 ± 2.8 mmol/kg, $p > 0.05$, unpaired t test). **d** Stool sodium concentrations of Nod2 k.o. animals were unchanged and not altered under Teduglutide treatment (mean ± SEM: day 0: 11.5 ± 4.2 mmol/kg vs. 8.0 ± 1.4 mmol/kg, $p > 0.05$, day 7: 11.8 ± 3.4 mmol/kg vs. 10.8 ± 2.7 mmol/kg, $p > 0.05$, day 14: 13.6 ± 4.8 mmol/kg vs. 12.1 ± 0.7 mmol/kg, $p > 0.05$, unpaired t test)

Teduglutide Improves Volume Status

Since aldosterone is secreted in response to salt and volume depletion [25], plasma aldosterone concentration was used as an indicator for volume status. Plasma aldosterone concentration at day 14 was significantly lower in Teduglutide-treated than in vehicle-treated wt animals (Fig. 3a). In Nod2 k.o. mice, plasma aldosterone concentrations were not significantly different between animals that received vehicle or Teduglutide. We have previously reported that Nod2 k.o. animals develop very high plasma aldosterone concentrations in this SBS model [11]. In line with that, two upward outliers occurred only in the vehicle-treated Nod2 k.o. group. In order to find out whether increased aldosterone concentrations reflect aldosterone action in the kidney, α-ENaC expression was analyzed in whole kidney lysates. Plasma aldosterone correlated linearly with kidney α-ENaC mRNA expression (Fig. 3b). In order to confirm ENaC localization, Aquaporin-2 (Aqp-2) was used as marker to histologically identify the aldosterone-sensitive distal nephron (ASDN) [25]. In line with the expression data, α-ENaC was located apically in the ASDN of vehicle-treated animals, while α-ENaC was located in the cytoplasm in the ASDN of Teduglutide-treated animals (Fig. 3c, d), reflecting enhanced compensatory aldosterone action in the kidney of vehicle-injected animals.

Teduglutide Maximizes Small Intestinal Mucosal Hypertrophy

Following small bowel resection, enhanced endogenous meal-stimulated GLP-1 and GLP-2 release from the colon likely contributes to the mucosal hypertrophy in the small bowel [26]. While the role of GLP-1 is less clear, GLP-2 is probably the inductor of this response in the small bowel [27]. In order to test how exogenous GLP-2 stimulation with Teduglutide affects this process, key parameters of adaptive intestinal hypertrophy were studied. In all groups, villus length was significantly increased 14 days after ICR (Fig. 4a). In wt mice, Teduglutide treatment significantly increased villus length even further, by additional 15% (293 ± 13 µm vs. 337 ± 21 µm, $p < 0.05$ Fig. 4b). Bowel diameter was unaffected by Teduglutide treatment (2351 ± 295 µm, vs. 2352 ± 146 µm, Fig. 4c) in wt mice. In Nod2 k.o. mice, villus length was significantly increased 14 days after ICR, and the effect from Teduglutide treatment was in the same numerical range as in wt animals, +17% (278 ± 17 µm vs. 326 ± 22 µm, $p = 0.09$). Interestingly, bowel diameter was increased in the resected Nod2 k.o. mice under both vehicle (2050 ± 59 µm vs. 2757 ± 465 µm $p < 0.05$) and Teduglutide treatment (1861 ± 92 µm vs. 2953 ± 373 µm, $p < 0.05$, Fig. 4c). Taken together, these data suggest that

Nod2 is not required for GLP-2-enhanced structural adaptation in the SBS situation.

Teduglutide Does Not Open the Tight Junction Leak Pathway

In order to study the tight junction leak pathway, the expression of tight junction genes, that modulate the tight junction leak pathway, Occludin, ZO-1, and ZO-2 [28, 29], was analyzed. Their expression levels were stable in the SBS situation (Fig. 5a, b) and not influenced by Teduglutide treatment ($p > 0.05$ for Teduglutide vs. vehicle, respectively). In the Ussing chamber, 4 kDa FITC dextran flux as an indicator for the leak pathway was determined [30]. In all resected groups, 4 kDa dextran flux was reduced, most likely due to the altered anatomy of the hypertrophied villi and independent of Teduglutide treatment and Nod2 status (Fig. 6). Taken together, flux via the leak pathway was not increased by Teduglutide and gene expression of the tight junction leak pathway regulator proteins Occludin, ZO-1, and ZO-2 was not reduced.

Teduglutide Improves Sodium Recirculation via Claudin-10

In order to find out whether Teduglutide impacts the tight junction pore pathway, biionic potentials were recorded in the Ussing chamber to assess size and charge selectivity. At day 0, there was a sharp size cutoff for permeability of cations between 2 and 3 Å, reflecting the high-capacity tight junction pore pathway [31]. This size cutoff was diminished at day 14 in vehicle-treated animals (Fig. 7a), while sodium selectivity as a marker for charge selectivity was maintained (Fig. 7c). In Teduglutide-treated wt animals, the size cutoff was restored at day 14 and sodium selectivity was significantly increased (Fig. 7a, c). In contrast, in Nod2 k.o. animals the size cutoff was lost after resection as in wt animals, but it was not reestablished by Teduglutide treatment (Fig. 7b). In addition, charge selectivity was significantly lower in the jejunum of Nod2 k.o. animals and not significantly increased by Teduglutide (Fig. 7d). In order to find out which component of the tight junction pore mediates this Nod2-dependent and Teduglutide-specific effect, mRNA expression of tight junction pore genes was analyzed (Figs. 8a, 9a). Claudin-2 expression was not significantly changed by Teduglutide treatment in wt mice. Both claudin-3 and claudin-7 tended to be increased after resection, but were unaffected by Teduglutide treatment. Also, claudin-4 expression was not different between the groups ($p > 0.05$, *U* test, Figs. 8a, 9a). Claudin-15 expression was changed to 2.8 ± 0.30-fold and 3.3 ± 0.44-fold, 14 days after ICR, again independent of Teduglutide treatment. This pattern was similar in Nod2 k.o. mice (Fig. 8a). Of note, only in wt mice, claudin-10 expression was significantly increased under Teduglutide compared to vehicle treatment (1.1 ± 0.24-fold vs. 0.55 ± 0.09-fold, $p < 0.05$, *U* test, Figs. 8a, 9a). Since claudin-10 promotes the tight junction cation pore in the intestinal epithelium [32], this is in line with the functional data which indicate maintained cation permeability in Teduglutide-treated animals.

Expression changes of tight junction genes may not necessarily result in functional changes of the tight junction because tight junction anchoring is required for pore formation [33]. Thus, we next studied claudin-10 localization along the crypt villus axis (Figs. 8b, c, 9c, d). Claudin-10 was localized in the tight junctions of the small bowel epithelium. However, in vehicle-treated wt mice, the claudin-10 immunofluorescence signal was lower in the villus tips (Fig. 9c, insets), while it was strong in the villus tips of Teduglutide-treated wt animals. Thus, in wt mice, Teduglutide promotes a paracellular cation pore that may be mediated by altered claudin-10 expression in the villus tip. Of note, this effect was absent in the Nod2 k.o. mice.

Function of the paracellular cation pore is important and beneficial for absorption because in the small intestine glucose is being absorbed electrogenically and transcellularly together with sodium by SGLT-1. Because there is more glucose to be absorbed than sodium, sodium is recircled paracellularly from the serosal to the luminal side by the pore properties of claudin-10. To facilitate efficient recirculation, Sglt-1 and claudin-10 need to be localized in the same villus compartment [34]. Thus, coimmunofluorescence was performed in wt mice. In vehicle-treated mice, the claudin-10 signal was weaker in the villus tips, while Sglt-1 signal was strong throughout the villi. But in Teduglutide-treated mice, claudin-10 signal was strong in the villus tips along with Sglt-1 signal (Fig. 9b).

Discussion

GLP-2 agonism is now an established treatment option for short bowel syndrome with intestinal failure [35, 36]. In patients, Teduglutide reduces parenteral hydration requirements, likely through improved water and electrolyte absorption [37–39]. Recent indirect evidence points to positive effects on nutrient absorption as well because parenteral energy supplementation can be reduced without body composition changes under Teduglutide therapy [40].

While the trophic effects on the small intestinal mucosa by GLP-2 stimulation are well described [40–43], the functional relevance of small bowel villus growth is less clear. The mechanistic implication of villus growth is called into question by translational observations: 1) Villus growth in response to Teduglutide is not in the same order of magnitude as a reduction of parenteral support (PS) [13], and

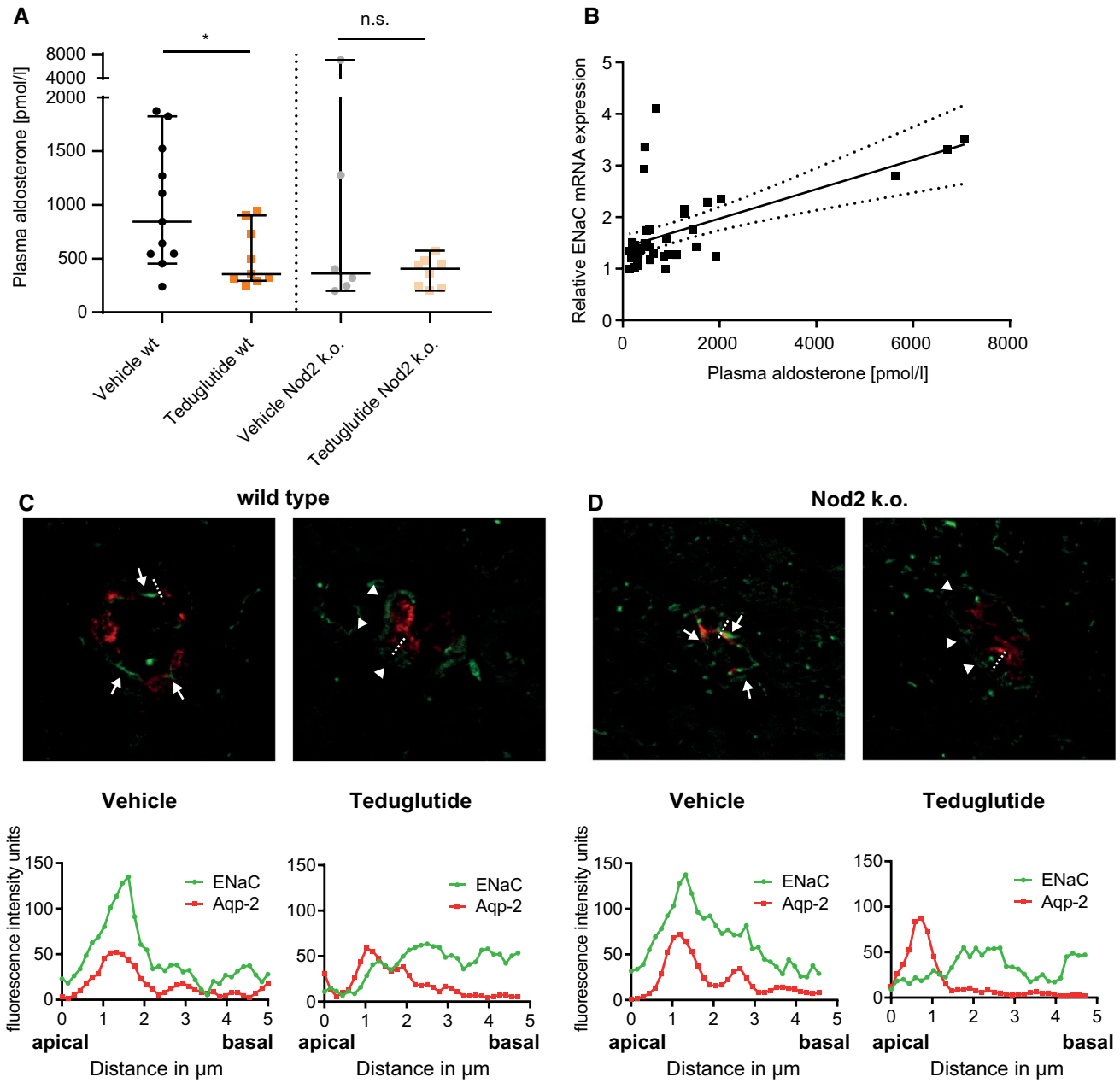

enterocyte mass expansion does not correlate with PS reduction [42]. 2) Body weight correlates negatively with villus length in the ICR mouse model [15]. 3) Structural disease, such as chronic obstruction, promotes villus growth but impairs absorption in the rat [44]. Thus, we set out to characterize specifically the functional effects of Teduglutide action on the small bowel epithelium in the SBS mouse model.

Due to the heterogeneity of the small human SBS cohort, mechanistic clinical studies are difficult to perform. Therefore, Teduglutide treatment was tested in the 14-day extensive ileocecal resection model in mice. This model represents the most common short bowel anatomy in humans and implies major loss of GLP-2 secretory capacity [18]. In this model, mice develop intestinal insufficiency, which they compensate by oral food intake. However, some mice develop IF with progressive weight loss and volume depletion leading to death [15]. Recent studies revealed that Nod2 dysfunction is a risk factor for IF in men and in mice [9, 11]. In mice, the absence of Nod2 in the SBS model is associated with barrier dysfunction and alterations in bacterial composition [11] possibly caused by altered bacterial sensing

◂**Fig. 3** Teduglutide improves volume status, indicated by reduced aldosterone action in the kidney. **a** Median plasma aldosterone concentration was measured at day 14. Aldosterone concentration was significantly lower in Teduglutide-treated compared to vehicle-treated wt mice (median ± 95% CI, $p < 0.05$, U test, $n = 11$ vs. $n = 9$). In Nod2 k.o. mice, no statistically significant difference was detectable, $p > 0.05$, U test, $n = 6$ versus $n = 8$. **b** Relative expression of ENaC on day 14 correlated with plasma aldosterone concentrations, across all groups, intention-to-treat population (Pearson's $r = 0.60$; $p < 0.5$, $n = 41$). **c** Upper panel: representative immunofluorescence of kidney collecting duct cells in Teduglutide- and vehicle-treated wt mice at day 14. Red: Aqp-2, green: α-ENaC. Of note, in vehicle-treated wt animals with high plasma aldosterone, localization was predominantly apical (white arrows). In Teduglutide-treated animals with low plasma aldosterone concentration, α-ENaC was localized in the cytoplasm (white arrowheads, no fluorescence peak in the line scan). Lower panel: Line scans through the apical membrane of collecting duct cells were performed. The red peak indicates the signal from Aqp-2 staining that was performed to label the apical membrane. In vehicle-treated wt mice, the green fluorescence peak converges with the red peak, suggesting colocalization of Aqp-2 with ENaC in the apical membrane and thus active ENaC. In Teduglutide-treated mice, the green signal peaked below the apical membrane, suggesting inactive ENaC. **d** Upper panel: representative immunofluorescence of kidney collecting duct cells in Teduglutide- and vehicle-treated Nod2 k.o. mice at day 14. Red: Aqp-2, green: α-ENaC. Of note, in vehicle-treated animals with high plasma aldosterone, localization was predominantly apical (white arrows). In Teduglutide-treated Nod2 k.o. animals with low plasma aldosterone concentration, α-ENaC was localized in the cytoplasm (white arrowheads, no fluorescence peak in the line scan). Lower panel: Line scans through the apical membrane of collecting duct cells were performed. The red peak indicates the signal from Aqp-2 staining that was performed to label the apical membrane. In vehicle-treated Nod2 k.o. mice, the green fluorescence peak converges with the red peak, suggesting colocalization of Aqp-2 with ENaC in the apical membrane and thus active ENaC. In Teduglutide-treated mice, the green signal peaked below the apical membrane, suggesting inactive ENaC

[45]. Therefore, we used wt mice as a model of intestinal insufficiency and Nod2 k.o. mice as a model of IF and tested the effects of Teduglutide on the outcome after extensive ileocecal resection.

In this model, vehicle-injected Nod2 k.o. mice had the highest incidence of IF. Strikingly, this negative effect of Nod2 deficiency on survival was reversed by Teduglutide treatment, supporting the notion that in humans Teduglutide is particularly efficient in severe IF [19]. It remains to be tested in clinical trials if NOD2 is an independent predictor for Teduglutide response in humans [46].

The fact that vehicle-treated Nod2 k.o. animals died early may have created an attrition bias in this cohort at day 14. Possibly, surviving mice in this cohort represent a form of positive selection, while the signal from the preterm dying mice could not be detected. This may have interfered with the mechanistic studies that were performed in the per protocol analysis for mice that reached day 14. In contrast, there was only a small dropout rate in wt animals, which allowed mechanistic interpretation of the data obtained in the per protocol analysis.

Compared to vehicle, Teduglutide treatment attenuated the persistent weight loss and thus intestinal insufficiency in wt mice. It is likely that improved body weight implies not only improved nutritional status but to some extent also improved volume status because fecal water losses were reduced and aldosterone concentrations as a marker of volume deficiency were improved by Teduglutide.

In order to quantify fecal losses, measurement of absolute stool volume and its composition would be the gold standard. However, the volume of watery and pasty diarrhea cannot reliably be quantified in absolute terms even with metabolic cages. Thus, as a marker for severity of diarrhea, we measured stool water content and sodium concentrations. Remarkably, stool water content was significantly reduced by Teduglutide, but stool sodium concentration was not significantly different between treatment groups. This indirectly suggests that in situations with high stool output, high sodium loss occurs as well and that Teduglutide reduces total stool sodium along with stool water loss. Although the effect of Teduglutide on stool water content appeared numerically small, it apparently translated to better volume status as indicated by less increased aldosterone concentrations. In addition, at day 2 stool water content was significantly increased after resection in all groups, but not significantly different between Teduglutide and vehicle-injected cohorts. The absence of a treatment effect by day 2 was likely due to the predominance of surgery-associated effects and the short treatment period up to this time point. In the late phase, e.g., at day 14, the effect of Teduglutide treatment on stool water reduction was also less pronounced, indicating that vehicle-treated mice adapted as well but slower and apparently through other mechanisms.

Aldosterone is the thirst hormone and regulates water and salt intake as well as excretion through the RAAS [47]. In vehicle-treated animals, plasma aldosterone concentrations were significantly higher compared to Teduglutide-treated animals. This indicates volume depletion secondary to the increased stool water and salt losses. In order to confirm RAAS activity, we studied α-ENaC expression in the kidney. Kidney α-ENaC mRNA expression correlated well with plasma aldosterone, indicating kidney-specific action of the systemically activated RAAS. Immunofluorescence for α-ENaC suggested that along with reduced aldosterone concentrations, Teduglutide reduced apical α-ENaC localization. Collectively, these data suggest that when *intestinal* adaptation is not sufficiently supported by Teduglutide, volume and salt depletion activate *systemic* mechanisms to counterregulate the fecal losses. Importantly, it is likely

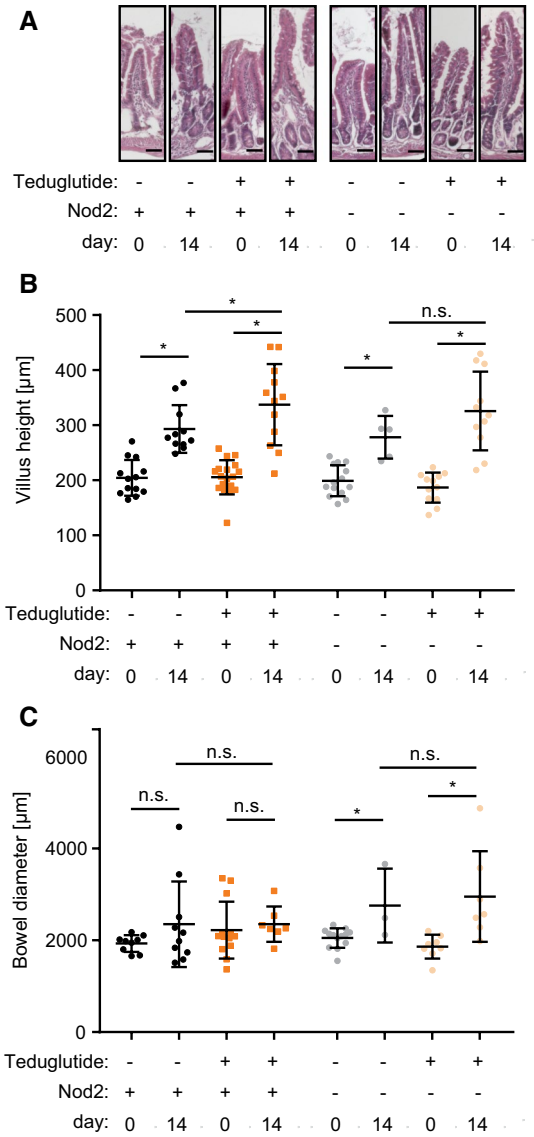

Fig. 4 Teduglutide influences structural hypertrophy. **a** Representative H.E. sections through jejunal villi. Scale bar represents 50 µm. **b** Villus length at day 0 and day 14. In wt animals, villus length was significantly increased by resection in vehicle-treated animals (day 0 vs. day 14: 204 ± 9.0 µm, $n = 13$ vs. 293 ± 13.0 µm, $n = 11$, $p < 0.05$, unpaired t test, mean ± SEM). Under Teduglutide treatment, villus length was even further increased (day 14 vehicle vs. Teduglutide: 293.1 ± 13.0 µm, $n = 11$ vs. 337 ± 21.3 µm, $n = 12$, $p < 0.05$, unpaired t test, mean ± SD). **c** Bowel diameter at day 0 and day 14. Bowel diameter was unaffected by Teduglutide treatment (2351 ± 295 µm, $n = 10$ vs. 2352 ± 146 µm, $n = 7$, $p > 0.05$, unpaired t test, mean ± SD)

that these systemic mechanisms may in turn activate colonic transport mechanisms as well.

In order to dissect the intestine-specific effects of Teduglutide, small bowel tissue was examined. ICR alone resulted in significantly increased villus length and crypt depth by ~ 50%, as seen in vehicle-treated animals and consistent with previous studies [48, 49]. In wt animals, Teduglutide significantly increased villus length further by ~ 15%. Remarkably, bowel diameter was unaffected by Teduglutide treatment, indicating the absence of horizontal small intestinal growth. While luminal expansion has been reported in mice in a long-term resection model [48], our observation is in line with clinical observations that small bowel diameter increases significantly only in ultrashort bowel syndrome [50]. Furthermore, small bowel dilatation may not be a direct result from loss of absorptive surface but instead indicate anastomotic stenosis or bowel paralysis. The absence of significant bowel distension in wt mice thus confirms the absence of such complications at day 14.

Because exogenous GLP-2 administration affects small bowel tight junction barrier in healthy mice [16], we tested the hypothesis that exogenous GLP-2 stimulation with Teduglutide effects the tight junction barrier in the SBS situation. The tight junction seals the paracellular space between enterocytes while creating a charge and size-selective mesh carrying both the leak and the pore pathway [51, 52]. The pore pathway is of particular physiologic relevance in the jejunum because it enables selective paracellular sodium recirculation and thus facilitates sodium, glucose, and water absorption, and we have previously shown that the paracellular tight junction pore to sodium is an important adaptive mechanism in the jejunum [15, 53]. A substantial contribution of the leak pathway, which facilitates passage of large uncharged solutes, must be excluded in order to study the pore pathway [30]. Indeed, the leak pathway was not impaired but even appeared tightened after resection, independent of Teduglutide treatment. This was paralleled by maintained gene expression of tight junction proteins that promote integrity of the leak pathway. While these data are in line with evidence that small bowel resection induces tightening of the paracellular barrier [54], they are apparently in contrast to evidence that resection loosens the paracellular barrier in the remnant epithelium [55]. To specifically address the tight junction pore pathway, we measured the tight junction cation size selectivity [56]. The paracellular pore pathway promotes bidirectional transport of ions [56]. While a portion of electrolyte absorption from luminal to basolateral occurs through this pathway, the pore also enables recirculation of sodium from basolateral to luminal to promote transcellular sodium-coupled nutrient transport via transporters such as SGLT-1 [57]. This sodium recirculation occurs via the cation-selective claudins in the jejunum and has been elegantly shown for claudin-15 in k.o. animals [34, 58].

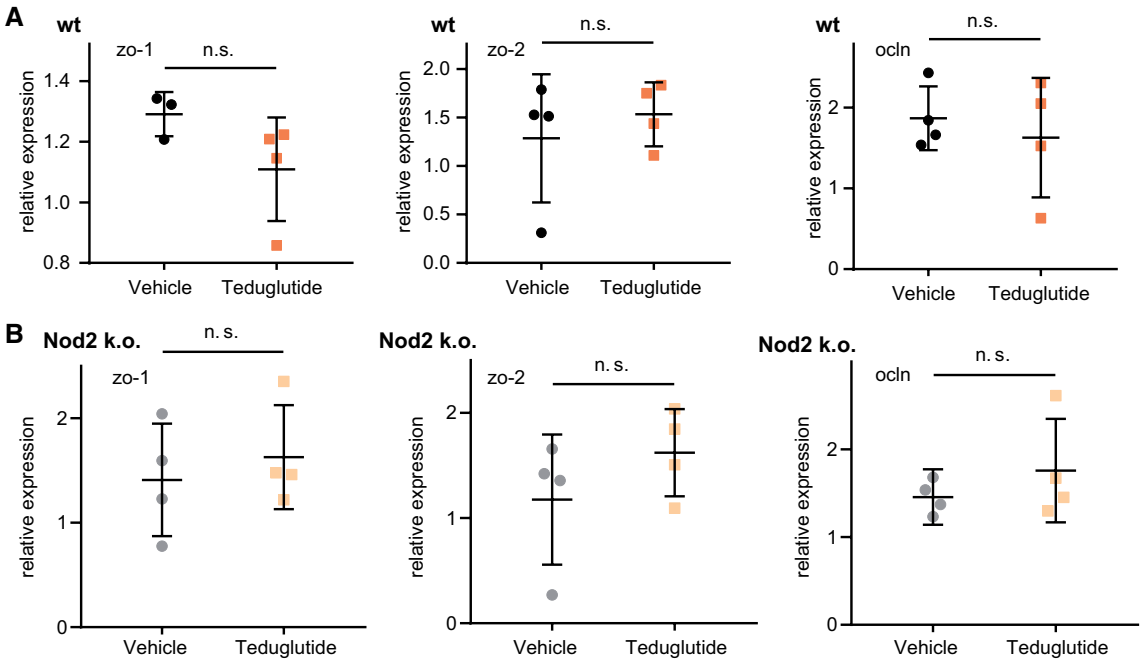

Fig. 5 Teduglutide effects on intestinal leak pathway tight junction genes relative to β-actin. **a** Expression change of tight junction leak pathway regulator genes ZO-1, ZO-2, and Occludin in wt animals, *U* test. **b** Expression change of tight junction leak pathway regulator genes ZO-1, ZO-2, and Occludin in Nod2 k.o. animals, *U* test

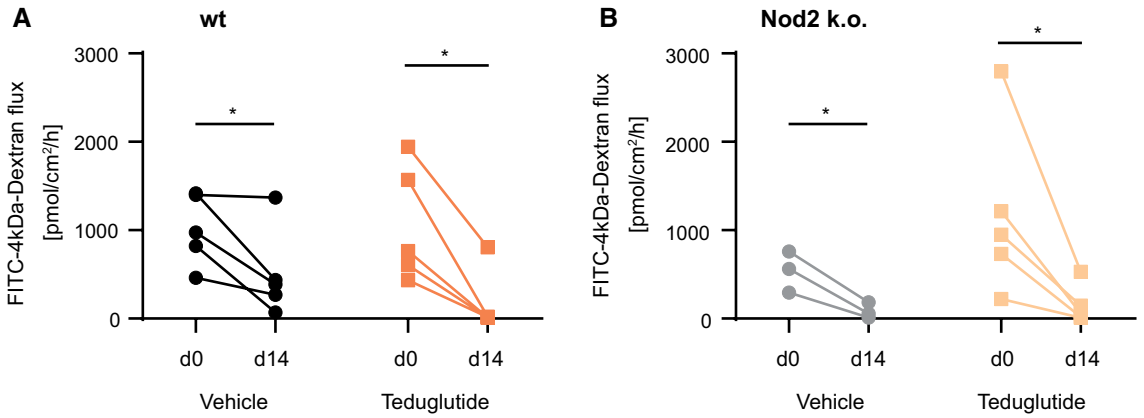

Fig. 6 Teduglutide does not promote the tight junction leak pathway. Absolute 4 kDa dextran permeability was measured in the Ussing chamber twice per mouse: at day 0 in the resected segment and at day 14 in the remaining "adjacent" segment. This approach allowed paired statistical testing. After resection, macromolecular permeability was significantly reduced, independent of Teduglutide or Nod2 status, paired *t* test, $p < 0.05$ in both wt (**a**) and Nod2 k.o. mice (**b**)

Paracellular cation size selectivity to small ions such as sodium was reduced in the SBS wt jejunum but maintained in the jejunum of the Teduglutide-treated wt cohort. Of note, for vehicle wt animals at day 14, a parallel shift in the curve was notable, which could be due to nonselective permeability changes from another unknown pathway that was not detected in the macromolecular permeability studies. If this shift was entirely due to enlarged intravillous tissue, one would expect even more a shift in the Teduglutide-treated wt mice at day 14. However, size selectivity was maintained in the maximally hypertrophied villi of the Teduglutide-treated mice. Furthermore, Teduglutide

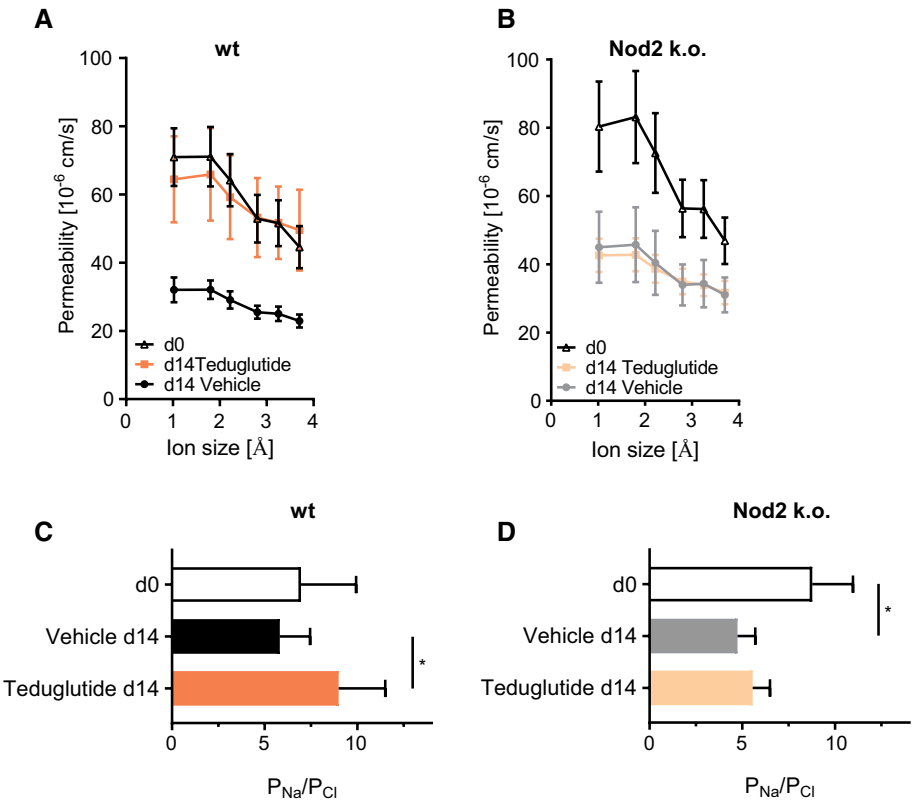

Fig. 7 Teduglutide promotes paracellular cation size selectivity in the SBS jejunum in wt mice. **a** Cation size selectivity in the jejunum is characterized by a size cutoff between 2 and 3 Å, which was detectable at day 0 in wt animals. In the adapted jejunum (d14 vehicle), this size cutoff seemed reduced. In contrast, under Teduglutide treatment, this size cutoff was preserved. Mean ± SEM. **b** In Nod2 k.o. animals, the tight junction size cutoff was similar to wt animals. At day 14, the size cutoff seemed lost in vehicle-treated animals but also in Teduglutide-treated animals. **c** Relative Na/Cl permeability in wt animals. P_{Na}/P_{Cl} was not significantly different between d0 and d14 (mean ± SD, $p > 0.05$, unpaired t test). Teduglutide treatment significantly increased P_{Na}/P_{Cl} (mean ± SD, $p < 0.05$, unpaired t test). **d** Relative Na/Cl permeability in Nod2 k.o. animals. P_{Na}/P_{Cl} was significantly lower at d14 compared to d0 (mean ± SD, $p < 0.05$, unpaired t test). Teduglutide had no effect on P_{Na}/P_{Cl} in Nod2 k.o. animals (mean ± SD, $p > 0.05$, unpaired t test)

promoted charge selectivity, i.e., P_{Na}/P_{Cl}, another measure for the tight junction pore specificity in the SBS jejunum [15]. These changes suggest that the paracellular claudin-based pore function in the jejunum is improved by Teduglutide.

In Nod2 k.o. animals, no effect of Teduglutide on pore function was observed, although resection alone also induced a parallel shift in the curve. The absence of an effect on the tight junction pore in Nod2 k.o. animals may be due to the lack of Nod2 signaling in the epithelium, although the pathway that connects Nod2 and GLP-2 has not been clarified yet. Also, attrition bias due to the significantly lower survival in the Nod2 k.o. vehicle cohort cannot be excluded.

Remarkably, claudin-10 expression was reduced in the vehicle treated but significantly increased in Teduglutide-treated wt animals. Of note, claudin-10 mRNA reduction was numerically small and it is well possible that the Teduglutide-dependent effect on the paracellular pore pathway is not purely due to claudin-10, but that there are other tight junction-dependent alterations at play in the intestine that were not detected in this study. Nevertheless, claudin-10 largely promotes the paracellular cation pore [32, 59]. Because only the claudin fraction that is inserted into the tight junction may participate in pore formation [60, 61], immunofluorescence was performed. Consistent with the previously described crypt-predominant expression of claudin-10 [62], the expression was higher near the crypts and

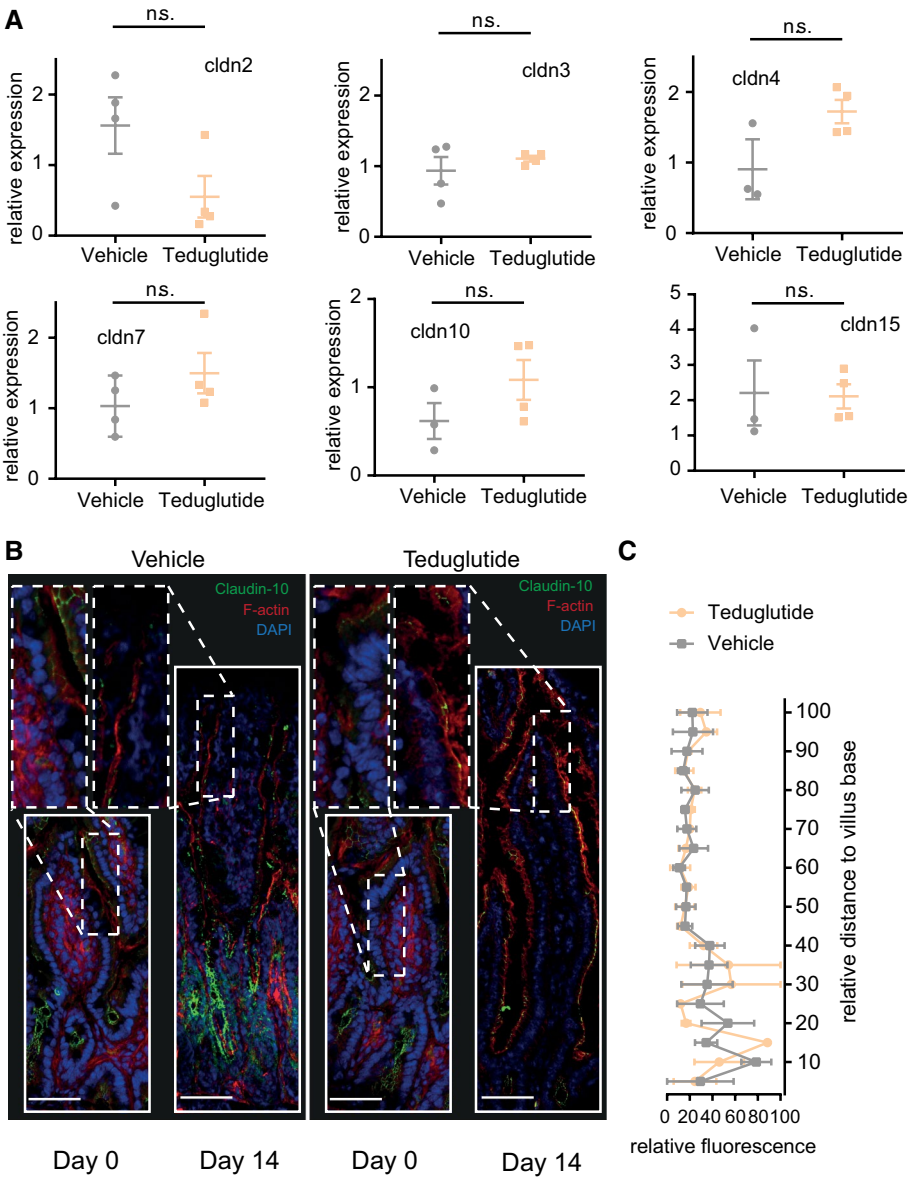

Fig. 8 Teduglutide has little effects in the Nod2 k.o. epithelium on claudin gene and protein function. **a** Expression of claudin mRNA in the small bowel epithelium. Values reflect $2^{-\Delta\Delta Ct}$ and are compared to day 0 and were normalized to β-actin. Mean ± SEM. $^{*}p < 0.05$, unpaired *t* test or Mann–Whitney *U* test. **b** Localization of claudin-10 along the villus length axis. Claudin-10 in green, F-actin in red, nuclei in blue. Scale bar: 50 µm. Claudin-10 signal was lost toward the villus tip in both vehicle- and Teduglutide-treated Nod 2 k.o. animals at day 14. Images represent the mean of 3 independent experiments per group. **c** Quantification of claudin-10 signal along the villus length axis, $n = 3$ per group. Mean ± SEM, two-way ANOVA, corrected for multiple testing with two-stage step-up method of Benjamini, Krieger, and Yekutieli

lower toward the villus tip in the small bowel under control conditions. This pattern was also present in the jejunum of vehicle-treated mice. In contrast, a strong claudin-10 signal was detected in the tight junction up to the villus tip in Teduglutide-treated mice. With semiquantitative immunofluorescence a significant difference was detectable specifically in the villus tips. This corresponds to the site of maximal SGLT-1 expression [63], suggesting that recirculation through the tight junction pore is mainly relevant in the villi and not at the villus base. From these data, we conclude that pharmacologic stimulation of adaptation with Teduglutide promotes paracellular sodium transport and thus facilitates enhanced sodium recirculation in order to promote sodium-coupled nutrient absorption, which in turn contributes to improved nutritional and volume status.

Taken together, this study shows (a) that Teduglutide alleviates intestinal insufficiency in wt mice and intestinal failure in Nod2 k.o. mice and (b) that these positive effects are accompanied by villus growth effects, but (c) that additional functional changes in the epithelium, such as paracellular pore selectivity, are involved in pharmacologic stimulation of absorption by Teduglutide.

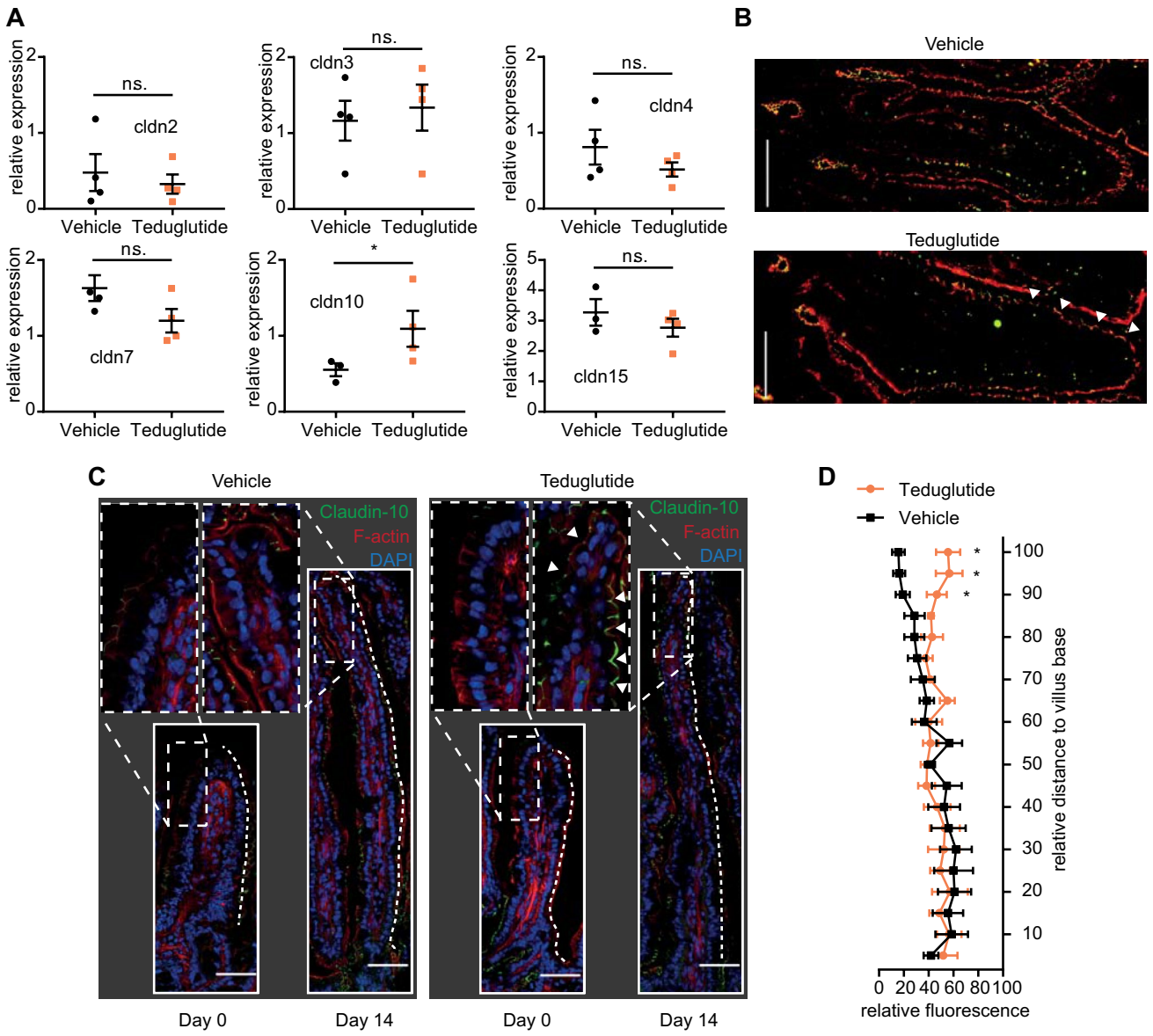

Fig. 9 Teduglutide promotes cation recirculation via claudin-10. **a** Expression of claudin mRNA in the small bowel epithelium. Values reflect $2^{-\Delta\Delta Ct}$ and are compared to day 0 and were normalized to β-actin. Mean ± SEM. *$p < 0.05$, unpaired *t* test or Mann–Whitney *U* test. **b** Immunofluorescence costaining of SGLT-1 (red) and claudin-10 (green) at day 14. Under both vehicle and Teduglutide treatment, SGLT-1 fluorescence was detected in the villous enterocytes. Under vehicle treatment, claudin-10 signal was lower in the villus tips. Under Teduglutide treatment, claudin-10 signal was strong in the villus tips (arrow heads). **c** Localization of claudin-10 along the villus length axis. Claudin-10 in green, F-actin in red, nuclei in blue. Scale bar: 50 µm. Claudin-10 signal was lost toward the villus tip in vehicle-treated animals at day 14. In contrast, claudin-10 signal was preserved up to the villus tip under Teduglutide treatment (arrow heads). Images represent the mean of 3 independent experiments per group. **d** Quantification of claudin-10 signal along the villus length axis, $n = 5–6$ per group. Mean ± SEM. *$p < 0.05$, two-way ANOVA, corrected for multiple testing with two-stage step-up method of Benjamini, Krieger, and Yekutieli

Acknowledgments Open Access funding provided by Projekt DEAL. We thank Julia Steinig and Katja Bergmann for excellent technical assistance. We appreciate Elisabeth Lamprecht for help with the stool analysis. We thank Prof. Ursula Seidler for critical discussion.

Funding This study was supported by an investigator-initiated research grant from Shire International GmbH, a member of the Takeda group of companies (# IIR-DE-000974). Johannes Reiner is a member of the Clinician Scientist Program funded by the University Medical Center Rostock. Peggy Berlin was supported by a grant from the Deutsche Forschungsgemeinschaft (BE 6292/1-1). Further funding was provided, through the research project "EnErGie", by the European Social Fund (ESF), reference: ESF/14-BM-A55-007/18, and the Ministry of Education, Science and Culture of Mecklenburg-Vorpommern.

Compliance with Ethical Standards

Conflict of interest Johannes Reiner and Georg Lamprecht received research support from Shire plc. for this study and from Zealand Pharma for unrelated research. For all other authors, no conflict of interest exists.

References

1. Pironi L, Arends J, Bozzetti F, et al. ESPEN guidelines on chronic intestinal failure in adults. *Clin Nutr*. 2016;35:247–307.
2. Warner BW. The pathogenesis of resection-associated intestinal adaptation. *Cell Mol Gastroenterol Hepatol*. 2016;2:429–438.
3. Seiler KM, Waye SE, Kong W, et al. Single-cell analysis reveals regional reprogramming during adaptation to massive small bowel resection in mice. *Cell Mol Gastroenterol Hepatol*. 2019;8:407–426.
4. Ladefoged K, Olgaard K. Fluid and electrolyte absorption and renin–angiotensin–aldosterone axis in patients with severe short-bowel syndrome. *Scand J Gastroenterol*. 1979;14:729–735.
5. Buchman AL, Scolapio J, Fryer J. AGA technical review on short bowel syndrome and intestinal transplantation. *Gastroenterology*. 2003;124:1111–1134.
6. Hampe J, Cuthbert A, Croucher PJ, et al. Association between insertion mutation in NOD2 gene and Crohn's disease in German and British populations. *Lancet*. 2001;357:1925–1928.
7. Ogura Y, Bonen DK, Inohara N, et al. A frameshift mutation in NOD2 associated with susceptibility to Crohn's disease. *Nature*. 2001;411:603–606.
8. Hugot JP, Chamaillard M, Zouali H, et al. Association of NOD2 leucine-rich repeat variants with susceptibility to Crohn's disease. *Nature*. 2001;411:599–603.
9. Schaffler H, Schneider N, Hsieh C-J, et al. NOD2 mutations are associated with the development of intestinal failure in the absence of Crohn's disease. *Clin Nutr*. 2013;32:1029–1035.
10. Ningappa M, Higgs BW, Weeks DE, et al. NOD2 gene polymorphism rs2066844 associates with need for combined liver-intestine transplantation in children with short-gut syndrome. *Am J Gastroenterol*. 2011;106:157–165.
11. Berlin P, Reiner J, Witte M, et al. Nod2 deficiency functionally impairs adaptation to short bowel syndrome via alterations of the epithelial barrier function. *Am J Physiol Gastrointest Liver Physiol*. 2019;317:G727–G738.
12. Drucker DJ. The discovery of GLP-2 and development of teduglutide for short bowel syndrome. *ACS Pharmacol Transl Sci*. 2019;2:134–142.
13. Jeppesen PB, Sanguinetti EL, Buchman A, et al. Teduglutide (ALX-0600), a dipeptidyl peptidase IV resistant glucagon-like peptide 2 analogue, improves intestinal function in short bowel syndrome patients. *Gut*. 2005;54:1224–1231.
14. Kaunitz JD, Akiba Y. Control of intestinal epithelial proliferation and differentiation: the microbiome, enteroendocrine L cells, telocytes, enteric nerves, and GLP, Too. *Dig Dis Sci*. 2019;64:2709–2716. https://doi.org/10.1007/s10620-019-05778-1.
15. Berlin P, Reiner J, Wobar J, et al. Villus growth, increased intestinal epithelial sodium selectivity, and hyperaldosteronism are mechanisms of adaptation in a murine model of short bowel syndrome. *Dig Dis Sci*. 2019;64:1158–1170. https://doi.org/10.1007/s10620-018-5420-x.
16. Dong CX, Zhao W, Solomon C, et al. The intestinal epithelial insulin-like growth factor-1 receptor links glucagon-like peptide-2 action to gut barrier function. *Endocrinology*. 2014;155:370–379.
17. Amiot A, Messing B, Corcos O, et al. Determinants of home parenteral nutrition dependence and survival of 268 patients with non-malignant short bowel syndrome. *Clin Nutr*. 2013;32:368–374.
18. Wewer Albrechtsen NJ, Kuhre RE, Torang S, et al. The intestinal distribution pattern of appetite- and glucose regulatory peptides in mice, rats and pigs. *BMC Res Notes*. 2016;9:60.
19. Jeppesen PB, Gabe SM, Seidner DL, et al. Factors associated with response to teduglutide in patients with short-bowel syndrome and intestinal failure. *Gastroenterology*. 2018;154:874–885.
20. Kobayashi KS, Chamaillard M, Ogura Y, et al. Nod2-dependent regulation of innate and adaptive immunity in the intestinal tract. *Science*. 2005;307:731–734.
21. Komen N, van der Wal H-C, Ditzel M, et al. Colorectal anastomotic leakage: a new experimental model. *J Surg Res*. 2009;155:7–12.
22. Rueden CT, Schindelin J, Hiner MC, et al. Image J2: ImageJ for the next generation of scientific image data. *BMC Bioinform*. 2017;18:529.
23. Reiner J, Hsieh C-J, Straarup C, et al. After intestinal transplantation kidney function is impaired by downregulation of epithelial ion transporters in the ileum. *Transplant Proc*. 2016;48:499–506.
24. Bodammer P, Kerkhoff C, Maletzki C, et al. Bovine colostrum increases pore-forming claudin-2 protein expression but paradoxically not ion permeability possibly by a change of the intestinal cytokine milieu. *PLoS ONE*. 2013;8:e64210.
25. Masilamani S, Kim GH, Mitchell C, et al. Aldosterone-mediated regulation of ENaC alpha, beta, and gamma subunit proteins in rat kidney. *J Clin Invest*. 1999;104:R19–R23.
26. Jeppesen PB, Hartmann B, Thulesen J, et al. Elevated plasma glucagon-like peptide 1 and 2 concentrations in ileum resected short bowel patients with a preserved colon. *Gut*. 2000;47:370–376.
27. Drucker DJ, Habener JF, Holst JJ. Discovery, characterization, and clinical development of the glucagon-like peptides. *J Clin Invest*. 2017;127:4217–4227.
28. Odenwald MA, Choi W, Kuo W-T, et al. The scaffolding protein ZO-1 coordinates actomyosin and epithelial apical specializations in vitro and in vivo. *J Biol Chem*. 2018;293:17317–17335.
29. Kuo W-T, Shen L, Zuo L, et al. Inflammation-induced occludin downregulation limits epithelial apoptosis by suppressing caspase-3 expression. *Gastroenterology*. 2019;157:1323–1337.
30. Tsai P-Y, Zhang B, He W-Q, et al. IL-22 upregulates epithelial claudin-2 to drive diarrhea and enteric pathogen clearance. *Cell Host Microbe*. 2017;21:671.e4–681.e4.
31. Samanta P, Wang Y, Fuladi S, et al. Molecular determination of claudin-15 organization and channel selectivity. *J Gen Physiol*. 2018;150:949–968.
32. Gunzel D, Yu ASL. Claudins and the modulation of tight junction permeability. *Physiol Rev*. 2013;93:525–569.

33. Raleigh DR, Boe DM, Yu D, et al. Occludin S408 phosphorylation regulates tight junction protein interactions and barrier function. *J Cell Biol*. 2011;193:565–582.
34. Wada M, Tamura A, Takahashi N, et al. Loss of claudins 2 and 15 from mice causes defects in paracellular Na+ flow and nutrient transport in gut and leads to death from malnutrition. *Gastroenterology*. 2013;144:369–380.
35. Jeppesen PB. The long road to the development of effective therapies for the short gut syndrome: a personal perspective. *Dig Dis Sci*. 2019;64:2717–2735. https://doi.org/10.1007/s10620-019-05779-0.
36. Naimi RM, Hvistendahl M, Enevoldsen LH, et al. Glepaglutide, a novel long-acting glucagon-like peptide-2 analogue, for patients with short bowel syndrome: a randomised phase 2 trial. *Lancet Gastroenterol Hepatol*. 2019;4:354–363.
37. Jeppesen PB, Gilroy R, Pertkiewicz M, et al. Randomised placebo-controlled trial of teduglutide in reducing parenteral nutrition and/or intravenous fluid requirements in patients with short bowel syndrome. *Gut*. 2011;60:902–914.
38. Seidner DL, Fujioka K, Boullata JI, et al. Reduction of parenteral nutrition and hydration support and safety with long-term teduglutide treatment in patients with short bowel syndrome-associated intestinal failure: STEPS-3 study. *Nutr Clin Pract*. 2018;33:520–527.
39. George AT, Li BH, Carroll RE. Off-label teduglutide therapy in non-intestinal failure patients with chronic malabsorption. *Dig Dis Sci*. 2019;64:1599–1603. https://doi.org/10.1007/s10620-019-5473-5.
40. Pevny S, Maasberg S, Rieger A, et al. Experience with teduglutide treatment for short bowel syndrome in clinical practice. *Clin Nutr*. 2019;38:1745–1755.
41. Drucker DJ, Erlich P, Asa SL, et al. Induction of intestinal epithelial proliferation by glucagon-like peptide 2. *Proc Natl Acad Sci USA*. 1996;93:7911–7916.
42. Seidner DL, Joly F, Youssef NN. Effect of teduglutide, a glucagon-like peptide 2 analog, on citrulline levels in patients with short bowel syndrome in two phase III randomized trials. *Clin Transl Gastroenterol*. 2015;6:e93.
43. Lai SW, de Heuvel E, Wallace LE, et al. Effects of exogenous glucagon-like peptide-2 and distal bowel resection on intestinal and systemic adaptive responses in rats. *PLoS ONE*. 2017;12:e0181453.
44. Bertoni S, Gabella G. Hypertrophy of mucosa and serosa in the obstructed intestine of rats. *J Anat*. 2001;199:725–734.
45. Schäffler H, Demircioglu DD, Kühner D, et al. NOD2 stimulation by Staphylococcus aureus-derived peptidoglycan is boosted by Toll-like receptor 2 costimulation with lipoproteins in dendritic cells. *Infect Immun*. 2014;82:4681–4688.
46. Witte MB. Reconstructive surgery for intestinal failure. *Visc Med*. 2019;35:312–319.
47. Rossier BC, Baker ME, Studer RA. Epithelial sodium transport and its control by aldosterone: the story of our internal environment revisited. *Physiol Rev*. 2015;95:297–340.
48. Dekaney CM, Fong JJ, Rigby RJ, et al. Expansion of intestinal stem cells associated with long-term adaptation following ileocecal resection in mice. *Am J Physiol Gastrointest Liver Physiol*. 2007;293:G1013–G1022.
49. Huang Y, Chen A, Guo F, et al. Severe intestinal dysbiosis in rat models of short bowel syndrome with ileocecal resection. *Dig Dis Sci*. 2020;65:431–441. https://doi.org/10.1007/s10620-019-05802-4.
50. Ives GC, Demehri FR, Sanchez R, et al. Small bowel diameter in short bowel syndrome as a predictive factor for achieving enteral autonomy. *J Pediatr*. 2016;178:275.e1–277.e1.
51. Shen L, Weber CR, Raleigh DR, et al. Tight junction pore and leak pathways: a dynamic duo. *Annu Rev Physiol*. 2011;73:283–309.
52. Furuse M, Furuse K, Sasaki H, et al. Conversion of zonulae occludentes from tight to leaky strand type by introducing claudin-2 into Madin-Darby canine kidney I cells. *J Cell Biol*. 2001;153:263–272.
53. Tamura A, Kitano Y, Hata M, et al. Megaintestine in claudin-15-deficient mice. *Gastroenterology*. 2008;134:523–534.
54. Bines JE, Taylor RG, Justice F, et al. Influence of diet complexity on intestinal adaptation following massive small bowel resection in a preclinical model. *J Gastroenterol Hepatol*. 2002;17:1170–1179.
55. Schulzke JD, Fromm M, Bentzel CJ, et al. Ion transport in the experimental short bowel syndrome of the rat. *Gastroenterology*. 1992;102:497–504.
56. Weber CR, Liang GH, Wang Y, et al. Claudin-2-dependent paracellular channels are dynamically gated. *Elife*. 2015;4:e09906.
57. Turner JR, Buschmann MM, Romero-Calvo I, et al. The role of molecular remodeling in differential regulation of tight junction permeability. *Semin Cell Dev Biol*. 2014;36:204–212.
58. Tamura A, Hayashi H, Imasato M, et al. Loss of claudin-15, but not claudin-2, causes Na+ deficiency and glucose malabsorption in mouse small intestine. *Gastroenterology*. 2011;140:913–923.
59. Gunzel D, Stuiver M, Kausalya PJ, et al. Claudin-10 exists in six alternatively spliced isoforms that exhibit distinct localization and function. *J Cell Sci*. 2009;122:1507–1517.
60. Weber CR, Turner JR. Dynamic modeling of the tight junction pore pathway. *Ann N Y Acad Sci*. 2017;1397:209–218.
61. van Itallie CM, Tietgens AJ, Anderson JM. Visualizing the dynamic coupling of claudin strands to the actin cytoskeleton through ZO-1. *Mol Biol Cell*. 2017;28:524–534.
62. Holmes JL, van Itallie CM, Rasmussen JE, et al. Claudin profiling in the mouse during postnatal intestinal development and along the gastrointestinal tract reveals complex expression patterns. *Gene Expr Patterns*. 2006;6:581–588.
63. Madunic IV, Breljak D, Karaica D, et al. Expression profiling and immunolocalization of Na(+)-D-glucose-cotransporter 1 in mice employing knockout mice as specificity control indicate novel locations and differences between mice and rats. *Pflugers Arch*. 2017;469:1545–1565.

Affiliations

Johannes Reiner[1] · Peggy Berlin[1] · Jakob Wobar[1] · Holger Schäffler[1] · Karen Bannert[1] · Manuela Bastian[2] · Brigitte Vollmar[3] · Robert Jaster[1] · Georg Lamprecht[1] · Maria Witte[4]

Johannes Reiner
johannes.reiner@med.uni-rostock.de

Peggy Berlin
peggy.berlin@uni-rostock.de

Jakob Wobar
jakob.wobar@uni-rostock.de

Holger Schäffler
holger.schaeffler@med.uni-rostock.de

Karen Bannert
karen.bannert@med.uni-rostock.de

Manuela Bastian
manuela.bastian@med.uni-rostock.de

Brigitte Vollmar
brigitte.vollmar@med.uni-rostock.de

Robert Jaster
robert.jaster@med.uni-rostock.de

Maria Witte
maria.witte@med.uni-rostock.de

[1] Division of Gastroenterology and Endocrinology, Department of Medicine II, Rostock University Medical Center, Ernst-Heydemann-Str. 6, 18057 Rostock, Germany

[2] Institute for Clinical Chemistry and Laboratory Medicine, Rostock University Medical Center, Ernst-Heydemann-Str. 6, 18057 Rostock, Germany

[3] Rudolf-Zenker-Institute of Experimental Surgery, Rostock University Medical Center, Schillingallee 69a, 18057 Rostock, Germany

[4] Department of General, Thoracic, Vascular and Transplantation Surgery, Rostock University Medical Center, Schillingallee 35, 18057 Rostock, Germany